(1)

AD-A223 199

DOCUMENTATION PAGE

Form Approved OMB No 0704-0188

UNCLASSIFIED	1b RESTRICTIVE MARKINGS
2a SECURITY CLASSIFICATION AUTHORITY	3 DISTRIBUTION/AVAILABILITY OF REPORT: Approved for public release; Distribution unlimited.
2b DECLASSIFICATION/DOWNGRADING SCHEDULE	
4 PERFORMING ORGANIZATION REPORT NUMBER(S): GL-TR-90-0142	5 MONITORING ORGANIZATION REPORT NUMBER(S)
6a NAME OF PERFORMING ORGANIZATION: Geophysics Laboratory (AFSC)	6b OFFICE SYMBOL (If applicable): OPI; 7a NAME OF MONITORING ORGANIZATION
6c ADDRESS (City, State, and ZIP Code): Hanscom AFB, Massachusetts 01731-5000	7b ADDRESS (City, State, and ZIP Code)
8a NAME OF FUNDING/SPONSORING ORGANIZATION	8b OFFICE SYMBOL (If applicable); 9 PROCUREMENT INSTRUMENT IDENTIFICATION NUMBER
8c ADDRESS (City, State, and ZIP Code)	10 SOURCE OF FUNDING NUMBERS

PROGRAM ELEMENT NO	PROJECT NO	TASK NO	WORK UNIT ACCESSION NO
61102F	2310	G4	23

11 TITLE (Include Security Classification): Vibrational relaxation of $OH(X^2\Pi_i, v=1-3)$ by O_2

12 PERSONAL AUTHOR(S): James A. Dodd, Steven J. Lipson, and William A.M. Blumberg

13a TYPE OF REPORT	13b TIME COVERED	14 DATE OF REPORT (Year, Month, Day)	15 PAGE COUNT
Reprint	FROM ____ TO ____	1990 June 12	7

16 SUPPLEMENTARY NOTATION: Reprinted from the Journal of Chemical Physics, Vol. 92, p. 3387

17 COSATI CODES		
FIELD	GROUP	SUB-GROUP

18 SUBJECT TERMS (Continue on reverse if necessary and identify by block number): Hydroxyl; OH; Collisional Relaxation; Oxygen; O_2

19 ABSTRACT (Continue on reverse if necessary and identify by block number)

Rate constants for $OH(X^2\Pi_i, v=1-3)$ vibrational relaxation induced by nonreactive collision with O_2 have been measured. $OH(v)$ is created by the $H + O_3 \rightarrow OH(v \leq 9) + O_2$ reaction in an electron-irradiated O_3, H_2, Ar mixture. $OH(v)$ fundamental and first overtone IR emission is observed using time-resolved Fourier spectroscopy. Spectral fitting followed by kinetic fitting of the resultant populations using a single-quantum relaxation model yields rate constants of $k_{v=1} = (1.3 \pm 0.4) \times 10^{-13}$, $k_{v=2} = (2.1 \pm 0.3) \times 10^{-13}$, $k_{v=3} = (2.9 \pm 0.8) \times 10^{-13}$ (all units are in cm^3/s). Our measurements are consistent with and extend published results on the same system, as well as predictions made by Schwartz–Slawsky–Herzfeld theory.

20 DISTRIBUTION/AVAILABILITY OF ABSTRACT	21 ABSTRACT SECURITY CLASSIFICATION
☐ UNCLASSIFIED/UNLIMITED ☒ SAME AS RPT ☐ DTIC USERS	UNCLASSIFIED

22a NAME OF RESPONSIBLE INDIVIDUAL	22b TELEPHONE (Include Area Code)	22c OFFICE SYMBOL
William A.M. Blumberg	(617)377-2810	GL(AFSC)/OPI

DD Form 1473, JUN 86 — Previous editions are obsolete. — SECURITY CLASSIFICATION OF THIS PAGE

UNCLASSIFIED

THE JOURNAL
OF
CHEMICAL PHYSICS

VOLUME 92 NUMBER 6

15 MARCH 1990

Vibrational relaxation of OH($X\ ^2\Pi_i$, $v=1$–3) by O_2

James A. Dodd, Steven J. Lipson, and William A. M. Blumberg
Geophysics Laboratory (AFSC)/OPI, Hanscom Air Force Base, Massachusetts 01731

(Received 3 October 1989; accepted 3 November 1989)

Published by the

AMERICAN INSTITUTE OF PHYSICS

Vibrational relaxation of OH($X\,^2\Pi_i$, $v=1$–3) by O_2

James A. Dodd, Steven J. Lipson, and William A. M. Blumberg
Geophysics Laboratory (AFSC)/OPI, Hanscom Air Force Base, Massachusetts 01731

(Received 8 August 1989; accepted 3 October 1989)

Rate constants for OH($X\,^2\Pi_i$, $v=1$–3) vibrational relaxation induced by nonreactive collision with O_2 have been measured. OH(v) is created by the $H + O_3 \rightarrow OH(v \leqslant 9) + O_2$ reaction in an electron-irradiated O_3, H_2, Ar mixture. OH(v) fundamental and first overtone IR emission is observed using time-resolved Fourier spectroscopy. Spectral fitting followed by kinetic fitting of the resultant populations using a single-quantum relaxation model yields rate constants of $k_{v=1} = (1.3 \pm 0.4) \times 10^{-13}$, $k_{v=2} = (2.1 \pm 0.3) \times 10^{-13}$, $k_{v=3} = (2.9 \pm 0.8) \times 10^{-13}$ (all units are in cm^3/s). Our measurements are consistent with and extend published results on the same system, as well as predictions made by Schwartz–Slawsky–Herzfeld theory.

INTRODUCTION

Hydroxyl radical (OH) plays a preeminent role in both the chemistry and photophysics of the earth's atmosphere. Stratospheric OH takes part in a number of key reactions, including those which determine the concentration of the halogen-containing species involved in the catalytic destruction of ozone.[1] OH also mediates the relative densities of the odd nitrogen oxides (NO and NO_2) and nitric acid. Because the presence of OH is a signature of numerous chemical and photochemical processes, its altitude distribution is of fundamental interest, and substantial effort has been made to develop better remote sensing techniques for OH.[2]

Meinel[3] first identified the intense nighttime emission in the near IR as arising from OH overtone transitions. The reaction between hydrogen atoms and ozone produces OH ($X\,^2\Pi, v$) in highly excited vibrational levels, with most of the nascent product distribution in $v = 7$–9, i.e., 21 500–26 200 cm^{-1} above the ground state (OH† will denote this species with $v \geqslant 1$). Unusually large probabilities for OH† multiquantum transitions give rise to the observed wideband emission. Theoretical and recent laboratory work has addressed the dearth of accurately known rovibrational Einstein coefficients for OH† IR fluorescence, which are necessary to determine populations from observed emission intensities.

The steady-state vibrational populations of hydroxyl in the upper atmosphere are determined by the rates of various processes, including the chemical reactions that form and destroy OH†, IR fluorescence from OH†, and collisional relaxation of OH† by bath gas molecules. At lower altitudes collisional relaxation becomes important, and accurate modeling of the atmosphere requires knowledge of the relevant rate constants, especially with the dominant molecular constituents. Much less is known, however, about the vibrational relaxation rates of OH† than about analogous rates of stable, closed-shell diatomic molecules, such as the hydrogen halides. In this report we address the relaxation of OH($v = 1$–3) upon nonreactive collision with oxygen molecules.

EXPERIMENT

All experiments were performed using the room-temperature LABCEDE apparatus, which has been described in detail.[4,5] A pulsed 35 kV electron beam excites a mixture of gases in a 5.4 liter, stainless-steel vacuum chamber ("target chamber"), pumped by a mechanical forepump. Differential pumping of the filament source region allows total pressures of up to 1 atm in the target chamber. Calibrated flow controllers (MKS 1258A; 1259B) and a 0–100 Torr range pressure transducer (MKS Baratron 220BA) were used to regulate gas flows and partial pressures.

OH† was produced by the reaction[6]

$$H + O_3 \rightarrow OH(v \leqslant 9) + O_2, \quad 2.8(-11)\ cm^3/s. \qquad (1)$$

[Hereafter rate constants are written in abbreviated form; e.g., in the above expression 2.8(−11) denotes 2.8×10^{-11}.] Ozone was formed using a commercial ozonator and stored on a column of silica gel at −78 °C. Prior to data-taking the column was purged of O_2 by pumping. Argon was subsequently flowed (35 sccm) through the column to entrain some of the adsorbed O_3 and pass it into the target chamber. Although we had no direct monitor for the ozone concentration in the target chamber, we estimate about 10^{14} molecules/cm^3 on the basis of the OH($v = 9$) formation rate (see below). The small flow of argon maintains this concentration of O_3 in the target chamber throughout the day; only a small fraction of the ozone on the column is actually used in the experiment.

The other precursor, H_2, is the source for the H atoms which react with O_3 molecules to form OH†. Both ozone (0.03% of the total number density) and hydrogen (1%) are diluted in an inert buffer gas, in this case argon. Thus, typical flow rates and pressures were as follows: Ar, 4000 sccm, 10 Torr; H_2, 60 sccm, 0.10 Torr; O_3, trace. In addition, up to 250 sccm (0.50 Torr) O_2 gas was added as a relaxer for OH†. Ultrahigh purity (99.999%) argon, hydrogen, and oxygen all were used without further purification. Impurity present in the added relaxer gas (oxygen) will result in at

 0021-9606/90/063387-07$03.00

most a 1% effect on the derived rate constants, assuming gas kinetic relaxation of OH† by the impurity.

The electron beam is pulsed on for 300 μs, then off for 19.7 ms to give a 1.5% gun duty cycle; observed current at the target chamber was 2–3 mA. The beam enters the target chamber through a pinhole orifice and is spread through elastic and inelastic collisions with the buffer gas. Some fraction of the energy lost by the beam results in molecular excitation. Intense fluorescence is seen in neat argon, both during the beam pulse and for several ms following pulse completion. When small amounts of ozone or oxygen are added, this fluorescence remains intense during the beam pulse, but is fully quenched 50 μs after the beam is turned off. When hydrogen is also present, OH† chemiluminescence dominates the IR emission following beam pulse termination.

A slow-scanning, room-temperature Michelson interferometer is used to observe the resultant OH† emission at 90° to the electron beam axis through a 6.35 cm diam CaF_2 window. The central fringe pattern is focused by a CaF_2 lens onto a 1.5 mm diam InSb detector cooled to 77 K. The detector responds from roughly 1.3 to 5.5 μ, D^* peaking near 5 μ. This region overlaps the fundamental and first overtone emission spectrum of OH†, and both sets of bands are evident in all of our spectral data. Spectra were obtained with 15–20 cm^{-1} resolution, which is the order of the rotational constant B in OH. OH† emission was sampled at 15–70 μs intervals, such that about 80 samples were used to characterize the total IR emission decay curve. The detector output was successively passed through a matched preamplifier (10× gain) and a PAR 113 preamplifier with 1 Hz low-frequency and 10 kHz high-frequency rolloff settings (50–200× gain), and then digitized.

The data-taking algorithm is described in detail elsewhere.[7] Helium–neon laser fringes are used as indicators of the relative mirror position. About 25 duty cycles of fluorescence decay information are averaged during each He–Ne $\lambda/2$ fringe; each fringe is scanned in 0.5 s in real time. Thus, a two-dimensional matrix of intensity as a function of fluorescence decay time and interferometer fringe position is built up over time. Typically, this matrix is composed of 80 time samples and 2000 mirror positions. Data are collected in real time by a Masscomp 5300 computer using 16 bit resolution, held in memory until completion of the scan, then transferred to an Apollo DN3000 computer. The Apollo is used to perform 16 K Fourier transforms on the raw, double-sided interferograms. Numerical phase correction methods[7] are used to generate real, time-ordered fluorescence spectra. Spectral fits were performed using a VAX 8650 computer (see next section).

Accurate correction of spectra for interferometer–detector spectral response was crucial, since the emission spans a wave number range in which the response varies by more than an order of magnitude. Calibration was accomplished using 1000 °C blackbody radiation, which was expanded with a CaF_2 telescope focused at infinity in order to fill the field of view directly in front of the interferometer opening. The calibration was performed under dry nitrogen to eliminate the effects of strong atmospheric absorbers (H_2O and CO_2). The curve obtained was insensitive to the precise placement of either the blackbody or the telescope. Identical calibration curves were obtained on two different days near the beginning and end of the study. Data were corrected directly prior to spectral fitting. A corrected spectrum is shown in Fig. 1.

SPECTRAL FITTING OF OH† FLUORESCENCE SPECTRA

Observed spectra show clear evidence of OH† emission from $v = 1$–9. It is well known from atmospheric and experimental observations that OH† has anomalously large first overtone transition probabilities.[8] Thus, all eight $v \rightarrow v-2$ transitions were observed in the overtone region, extending roughly from 4200 to 7200 cm^{-1}. The fundamental bands with $v' \geqslant 6$ are embedded in the noise of our spectra, however, even though they occur in a region where the detector is most sensitive (1800 to 2800 cm^{-1}). All spectra were fit in the wave number range 2500 to 7300 cm^{-1}.

Accurate spectral fitting of OH† vibrational emission spectra requires knowledge of both rovibrational frequencies and Einstein coefficients. Spin-rotational term values for $v \leqslant 10$ accurate to a few hundredths of a cm^{-1} have been published.[9,10] Mies[11] and Langhoff, Werner, and Rosmus[12] have reported detailed computations of theoretical transition probabilities for OH† rovibrational lines for $v' = 1$–9, $\Delta v = 1$–5. Very recently, Turnbull and Lowe[13] published values based on an empirical dipole moment function for OH, while Nelson *et al.*[14] reported values obtained through a direct measurement of OH† transition probabilities using both absorption and emission spectroscopy. At this time, however, certain important aspects of OH† emission remain controversial, notably the relative vibrational band intensi-

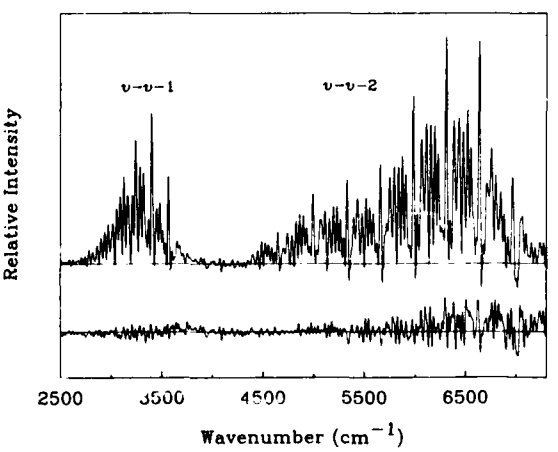

FIG. 1. Typical observed OH† emission spectrum, corrected for spectral response. Note the prominent Q branches in the overtone region for $v' = 2$–9. Residuals from the spectral fit are shown offset beneath the spectrum; zero lines are included for both plots. Statistical weighting of data points in the fit causes the larger residuals evident at larger wave number (see text). Pressures used: 10.1 Torr Ar, 0.10 Torr H_2, 0.003 Torr O_3. e-beam parameters: 35.0 kV, 2.55 mA at the target chamber, 0.3 ms duration, 19.7 ms between pulses. Spectrum was taken 0.3 ms after beam termination.

ties.[15] As discussed below, this issue does not have a large impact on our analysis.

In order to spectrally fit observed data, tabulated intensities must be multiplied by initial-state populations, and the lines then convolved with the interferometer line-shape function. Under our experimental conditions collisions occur on a time scale (0.1 μs) much shorter than the fluorescence decay times, suggesting a steady-state Boltzmann distribution of rotational states at each v level. The line-shape function is conveniently written as a function of two parameters: the FWHM linewidth Δ, and a parameter α which describes the line shape. The interferometer output over 2000 fringes using an extended, monochromatic helium lamp source can be approximated as a linear combination of an unapodized and a triangularly apodized interferogram. Fourier transformation of such an interferogram gives a spectral line described by a linear combination of the sinc and sinc^2 functions.[16] The parameter α specifies the fraction of the sinc function in the superposition.

Vibrational populations were determined through linear least-squares fits to the spectra, using basis functions obtained by convolving Boltzmann-weighted line strengths with the instrument line-shape function. The factors which multiply each of the nine vibrational basis functions in the best-fit result are the relative populations. Best values for Δ, α, and T are obtained through nonlinear fits to selected spectra for a given day's data. These parameters are then fixed, and basis functions are computed for the far less time-consuming linear fits for the populations. Δ, α, and T do not vary more than a few percent over the course of the day, and the variation does not appreciably affect the best-fit values of the populations. Typically, $\Delta = 16$–$19\ \mathrm{cm}^{-1}$ (depending on how many interferogram fringes are used), $\alpha = 0.75$, and $T = 300$ K, i.e., room temperature. No evidence is seen at any time in the fluorescence decay of a nonthermal distribution of rotational states.

Spectra not corrected for detector response show equal noise at all wave-number values; division by the spectral correction function results in a noise level which increases with wave number. Thus, points were statistically weighted as the inverse of the spectral correction function in the linear fits, placing more importance on data near the red end of the spectrum where the detector is most sensitive.

Both the Mies and Langhoff *et al.* sets of Einstein coefficients yield good spectral fits of our data, as measured by the value of "Q" resulting from the fitting program.[17] In addition, the derived rate constants did not change significantly when one or the other set of Einstein coefficients was used. Because our derived rate constants are insensitive to the choice of Einstein coefficient data set, the Mies and Langhoff *et al.* data sets were used interchangeably in analyzing OH† spectral data.

KINETIC MODEL FOR FITTING OF POPULATION DECAYS: RELEVANT CHEMISTRY

The spectral fits produce a family of population decay curves, with $v_{max} = 9$. Figure 2 shows such a family of curves for the four lowest levels; the populations in $v = 5$–9 are smaller and have been omitted for clarity. Ideally, this data is least-squares fit to determine the rates describing all OH† single and multiquantum relaxation processes. However, severely imprecise and correlated kinetic parameters result when any subset containing n curves is fit using more than n adjustable parameters. Because we are unable to determine all of the decay rates, we use the most salient model which incorporates one rate for each v level, i.e., that which allows single-quantum relaxation only. Clearly, this model may fail due to two mechanisms not taken into account: (1) multiquantum relaxation and (2) chemical quenching, which removes OH† from the v ladder altogether. We now present evidence supporting the validity of our simplified model.

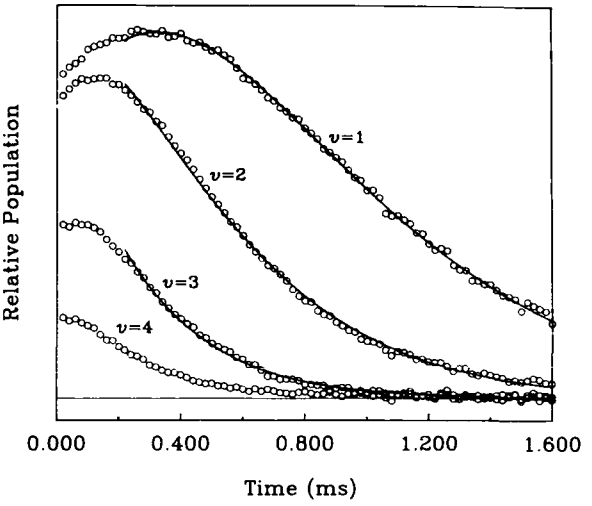

FIG. 2. Observed population decay curves for OH($v = 1$–4), derived from spectral fits. Also shown is a kinetic fit to $v = 1$–3 with $v = 4$ as an empirical feed. Poorer fits result if populations immediately after beam termination (time $t = 0$) are included. At early times rapidly cascading upper v states and/or H atoms produce conditions which violate the single-quantum decay model (see text).

Little is known about the detailed behavior of vibrationally excited OH† upon collision with relaxer molecules. Modeling studies[18,19] of state-to-state cross sections for OH(v,J) collisions with Ar atoms, however, suggest that multiquantum relaxation is important for $v = 9$, but not important for $v = 1$–4. These studies suggest that the single-quantum mechanism will model the low v levels better than the high v levels.

Two kinds of species which chemically quench OH† need to be considered: those which are flowed through the apparatus continuously, and those which are created by the action of the electron beam. In the first category, only ozone reacts with OH† with a rate that may be significant:

$$\mathrm{OH} + \mathrm{H_2} \rightarrow \mathrm{H} + \mathrm{H_2O}, \quad 6.3(-15)\ \mathrm{cm^3/s} \quad (20\ \mathrm{s^{-1}}\ \text{at}\ 0.10\ \text{Torr}\ \mathrm{H_2}), \tag{2}$$

$$\mathrm{OH} + \mathrm{O_2} \rightarrow \text{products}, \quad \text{very slow}, \tag{3}$$

$$\mathrm{OH}(v = 0) + \mathrm{O_3} \rightarrow \mathrm{HO_2} + \mathrm{O_2}, \quad 6.7(-14)\ \mathrm{cm^3/s} \quad (6\ \mathrm{s^{-1}}\ \text{at}\ 0.003\ \text{Torr}\ \mathrm{O_3}), \tag{4}$$

$$\mathrm{OH}(v \geq 1) + \mathrm{O_3} \rightarrow \mathrm{H} + 2\mathrm{O_2} \tag{5a}$$

$$OH(v \geqslant 3) + O_3 \rightarrow OH(v') + O + O_2, \quad (5b)$$

$$OH(v = 9) + O_3 \rightarrow \text{products}, \quad 2.0(-10)\ \text{cm}^3/\text{s} \quad (18\,000\ \text{s}^{-1}\ \text{at}\ 0.003\ \text{Torr}\ O_3). \quad (5c)$$

Two different reports[20,21] have indicated that the reaction of OH(9) with O_3 is very rapid. The rate constants for the detailed set of OH/O_3 reactions indicated above have not been determined for $1 \leqslant v \leqslant 8$. However, new channels open up with increasing excitation of OH. In addition to the above reactions, for instance, the channel

$$OH(v) + O_2 \rightarrow HO_2 + O \quad (6)$$

is energetically feasible for $v \geqslant 6$. Since the lower v levels would be expected to have longer reactive lifetimes, they should be more accurately fit by the single-quantum relaxation model. Due to its numerous reactions with $OH^\dagger$, the concentration of O_3 was minimized consistent with S/N requirements.

Species which are created by the electron beam often cannot be observed directly, but must be identified from considerations of the reaction chemistry. Ions formed during the beam pulse recombine with electrons on a time scale which is short compared to that of OH fluorescence decay.[22] Atoms, in this case H and O, pose a more serious problem. Hydrogen atoms in all likelihood are very efficient multiquantum relaxers of $OH^\dagger$, operating through an atom exchange mechanism.[23] However, H atoms have a lifetime following beam pulse termination which is limited by the O_3 concentration,

$$H + O_3 \rightarrow OH^\dagger + O_2, \quad 2.8(-11)\ \text{cm}^3/\text{s} \quad (2600\ \text{s}^{-1}\ \text{at}\ 0.003\ \text{Torr}\ O_3). \quad (1')$$

Thus, one allows the H-atom population to decay before analyzing the $OH^\dagger$ fluorescence (see below).

As discussed in the literature[20,24] OH(9) reacts with O_3 ten times faster than it is produced by the $H + O_3$ reaction. Greenblatt and Wiesenfeld,[20] working under pressure conditions similar to those reported here, found the decay rate for $OH(v = 9)$ to be independent of bath gas pressure, and identified the rate associated with the decay to $OH^\dagger$ formation, not relaxation. We observe also that the $OH(v = 9)$ fluorescence decay rate is independent of bath gas pressure. Thus, we identify the fluorescence decay of $OH(v = 9)$ with the decay of H-atom precursor. Consistent with this identification, we obtain much better fits for the kinetic behavior of $OH(v = 1\text{–}3)$ by first allowing $OH(v = 9)$ fluorescence to decay. In addition, one can estimate the O_3 concentration by dividing the observed $OH(v = 9)$ decay rate by the rate constant given in reaction (1). The decay rate of 2600 s^{-1} leads to the reported pressure of 0.003 Torr O_3.

Unlike H atoms, ground-state $O(^3P)$ does not react quickly with any of the molecules present with the exception of OH:

$$O + H_2 \rightarrow OH + H, \quad \text{very slow}, \quad (7)$$

$$O + O_3 \rightarrow 2O_2, \quad 8.0(-15)\ \text{cm}^3/\text{s} \quad (1\ \text{s}^{-1}\ \text{at}\ 0.003\ \text{Torr}\ O_3), \quad (8)$$

$$O + OH \rightarrow O_2 + H, \quad 3.9(-11)\ \text{cm}^3/\text{s}. \quad (9)$$

Reaction (9) generates H atoms from ground-state OH, which in turn react with O_3 *via* reaction (1) to regenerate OH ($v \leqslant 9$). This delayed feed mechanism severely complicates the kinetics. If high concentrations of O exist in the cell, the observed rates are lower than the true relaxation rates due to this delayed feed. Anomalously low relaxation rates were observed when (1) the gun duty cycle was increased from 1.5% to 3%, and (2) the O_2 pressure was increased above about 0.5 Torr, at which point the Stern–Volmer plot of rate vs O_2 pressure takes on negative curvature.

The effect of increasing the beam-on time is to produce more of all beam-created species, the steady-state populations of which are complex functions of their creation, quenching, and pump-out rates. Two instrumental time scales of note are the residence time in the field of view of the interferometer (0.1 s) and in the target chamber as a whole (1 s). These time scales are longer than the $OH^\dagger$ fluorescence decay (5 ms) and duty cycle (20 ms) times. Thus, long-lived species may play a significant role in $OH^\dagger$ quenching. For instance, if the OH concentration is too high self-degradation reactions become important:

$$OH + OH(v) \rightarrow OH + OH(v'), \quad (10)$$

$$OH + OH \rightarrow O + H_2O, \quad 2.0(-12)\ \text{cm}^3/\text{s}. \quad (11)$$

To guard against quenching by beam-created species, one either (1) extrapolates rates observed at two or more pulse widths to zero pulse width, or (2) demonstrates that the rates do not depend on pulse width. The latter approach was used here; no dependence of the rates was found as a function of pulse width from 250–350 μs. A pulse width of 300 μs was used in most of the experiments.

The effect of O_2 pressure on O-atom density can be understood by considering the chemistry of the $Ar/H_2/O_3/O_2$ system under e-beam excitation. High energy excitation of this gas mixture produces H atoms, as well as O atoms in the ^3P and ^1D states. H reacts with O_3 *via* reaction (1) to produce $OH^\dagger$ in highly excited vibrational states. Any $O(^1D)$ present during the e-beam is quickly quenched after e-beam turn-off, either by reaction with H_2 to produce $OH^\dagger$ in low v ($v \leqslant 4$ is energetically allowed) and high J,[25]

$$O(^1D) + H_2 \rightarrow OH^\dagger + H \quad 3(-10)\ \text{cm}^3/\text{s} \quad (960\,000\ \text{s}^{-1}\ \text{at}\ 0.10\ \text{Torr}\ H_2) \quad (12)$$

or by collision with Ar atoms[26] or O_2 molecules,[27]

$$O(^1D) + Ar \rightarrow O(^3P) + Ar, \quad 3.6(-13)\ \text{cm}^3/\text{s} \quad (115\,000\ \text{s}^{-1}\ \text{at}\ 10.0\ \text{Torr Ar}), \quad (13)$$

$$O(^1D) + O_2 \rightarrow O(^3P) + O_2, \quad 2.4(-11)\ \text{cm}^3/\text{s} \quad (370\,000)\ \text{s}^{-1}\ \text{at}\ 0.5\ \text{Torr}\ O_2). \quad (14)$$

$O(^3P)$ densities increase at higher O_2 pressure, due to a faster production rate from O_2 and increased quenching *via* reaction (14). Thus, to avoid the delayed feed mechanism discussed above, we derive the $OH^\dagger/O_2$ relaxation rate constant in the O_2 pressure regime where the slope of the Stern–Volmer plot is linear, and the rates do not depend on pulse width.

In terms of the kinetic analysis, clearly the levels which

are fed directly by reaction (1) ($v = 6$–9) cannot be described by our single-quantum relaxation model. Even if a single-quantum relaxation mechanism were operative for all v, which seems doubtful, our model would fail because the observed fluorescence decay for higher v describes a formation rate; therefore, the fluorescence for these v levels cannot be used to extract relaxation rate information. To analyze the relaxation kinetics for high v a different source must be used.

Because of the problems with the upper v levels, we decided to concentrate on the lower v. In order to provide a (necessary) feed term for the highest v level in the fit, we use the observed decay of a level v_j as an empirical feed term for the level directly below it. In so doing we remove v_j from the set of levels being fit, in addition to all levels above v_j. In order to fit as many levels as possible, we choose v_f as the highest level for which the feed model produces acceptable fits. We assume negligible feed into all $v < v_f$ from all levels above v_f, and that all $v \leq v_f$ decay by the single-quantum mechanism. We are able to fit $v = 1$–3 very well using this technique, with $v = 4$ decay providing the empirical feed term.

The relevant kinetic processes included in our model are given by

$$\mathrm{OH}(v) + \mathrm{O_2} \rightarrow \mathrm{OH}(v-1) + \mathrm{O_2}, \quad k(v),$$

$$\mathrm{OH}(v) + M \rightarrow \mathrm{OH}(v-1) + M, \quad k_M(v),$$

$$\mathrm{OH}(v) \rightarrow \mathrm{OH}(v-1) + h\nu, \quad A_{v,v-1},$$

$$\mathrm{OH}(v) \rightarrow \mathrm{OH}(v-2) + h\nu', \quad A_{v,v-2}.$$

The rate constants $k(v)$ describe single-quantum relaxation of $\mathrm{OH}(v)$ by $\mathrm{O_2}$, the rate constants k_M describe relaxation by molecules other than $\mathrm{O_2}$ (e.g., Ar), and the radiative rates A_{ij} are for $v = i \rightarrow v = j$. Rates R which do not depend on $[\mathrm{O_2}]$ can be grouped together, *viz.*

$$R(1) = k_M(1)[M] + A_{10},$$

$$R(2) = k_M(2)[M] + A_{21},$$

$$R'(2) = R(2) + A_{20},$$

$$R(3) = k_M(3)[M] + A_{32},$$

$$R'(3) = R(3) + A_{31}.$$

Thus, the differential equations describing the time dependence of the populations are written

$$\frac{d[\mathrm{OH}(1)]}{dt} = -\{R(1) + k(1)[\mathrm{O_2}]\}[\mathrm{OH}(1)] + \{R(2) + k(2)[\mathrm{O_2}]\}[\mathrm{OH}(2)] + A_{31}[\mathrm{OH}(3)],$$

$$\frac{d[\mathrm{OH}(2)]}{dt} = -\{R'(2) + k(2)[\mathrm{O_2}]\}[\mathrm{OH}(2)] + \{R(3) + k(3)[\mathrm{O_2}]\}[\mathrm{OH}(3)],$$

$$\frac{d[\mathrm{OH}(3)]}{dt} = -\{R'(3) + k(3)[\mathrm{O_2}]\}[\mathrm{OH}(3)] - \frac{d[\mathrm{OH}(4)]}{dt}_{\mathrm{obs}}.$$

The A_{ij} are about 2 orders of magnitude smaller than the collisional relaxation rates: the three-quantum Einstein coefficients are negligible. The argon bath gas gives rise to a y intercept in the Stern–Volmer plot of about one-third of the maximum rate increase due to added relaxer $\mathrm{O_2}$.

We solve these coupled linear differential equations numerically by estimating initial values for the decay rates, then integrating the equations over the time of the experimental observations to produce model curves for $v = 1$–3. A nonlinear least-squares-fitting routine then iteratively adjusts the rates to produce the best least-squares fit to the experimental data, and in so doing determines the best values of the rate parameters. Typically 50–80 time points for each v level are fit in this manner for each run, and several runs are taken at each relaxer pressure. Stern–Volmer plots are then constructed from the various pressures; a plot from one experiment is shown in Fig. 3. The slope of the Stern–Volmer plot determines the rate constant for relaxation of OH† by $\mathrm{O_2}$. The intercept (typically 1500–2000 $\mathrm{s^{-1}}$) indicates the relaxation rate which is due primarily to the buffer gas. Many days of data were analyzed, and the rate constants averaged to produce the rate constants reported herein.

RESULTS AND DISCUSSION

Rate constants derived for OH† relaxation by $\mathrm{O_2}$ are presented in Table I. We include in the table two previous measurements of OH† /$\mathrm{O_2}$ relaxation rate constants; both are consistent with the present measurements. Jaffer and Smith[28] could only obtain an upper bound for the $v = 1$ rate in their flow tube experiment. In a more recent experiment, Rensberger, Jeffries, and Crosley[29] obtained the total rate for *relaxation from* OH(2) initially populated by a laser tuned to various rotational lines in the 2–0 band. They did not determine the relative importance of the single- vs double-quantum pathways in their experiment. However, the fact that their value agrees with our value arising from a single-quantum mechanism suggests that single-quantum relaxation is more important than double-quantum relaxation.

Streit and Johnston[30] report values for OH† relaxation

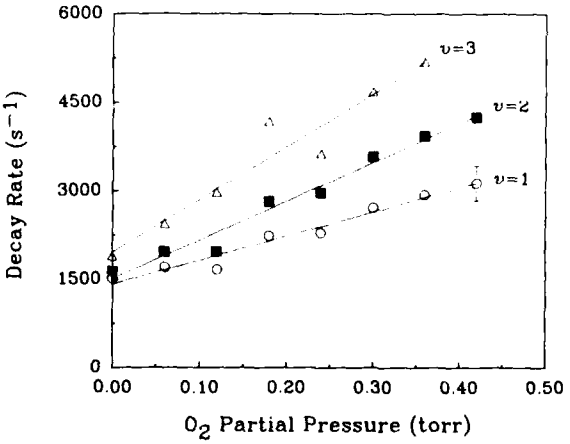

FIG. 3. Dependence of the decay rates for OH(v = 1–3) upon $\mathrm{O_2}$ pressure for one day's data. Nonzero y intercepts are due primarily to bath-gas-induced relaxation.

TABLE I. Rate constants for $OH(X\,^2\Pi_i, v) + O_2 \rightarrow OH(v-1) + O_2$.

	Rate constant[a] (10^{-13} cm^3/s)	
v	Present result	Literature
1	1.3 ± 0.4	< 4[b]
2	2.1 ± 0.3	2.6 ± 0.4[c]
3	2.9 ± 0.8	

[a] All uncertainties are 2σ.
[b] Reference 28.
[c] Reference 29. Measurement is the rate constant for total collisionally induced loss out of $v = 2$.

by O_2 for $v = 4$–9 in the mid-10^{-13} cm^3/s range, using a kinetic model which assumes single-quantum relaxation for all v levels. That work has been strongly questioned,[24] both because of the complications described above in the analysis of the upper v, and also because incorrect Einstein coefficients were used. Finlayson-Pitts and Kleindienst[24] report a rate constant for the removal of OH(9) by O_2 of 1×10^{-11} cm^3/s, assuming the Mies[11] value for the $A_{9,1}$ Einstein coefficient. Their result is consistent with the values reported here for lower v, although obviously more work needs to be done to determine rate constants for intermediate v.

There have been numerous measurements of the rates of vibrational relaxation in $OH(A\,^2\Sigma^+)$ by O_2.[31] For O_2 as well as for a number of other relaxers, such rates are 2 orders of magnitude larger than the corresponding values for $OH(X\,^2\Pi_i)$. Rensberger, Jeffries, and Crosley[24] suggest that $OH(A)$-relaxer collision complexes have stronger binding energies than their $OH(X)$ counterparts, allowing more efficient energy transfer. A more strongly bound complex would be expected to give rise to more multiquantum relaxation of $OH(v)$. German,[32] however, studying the relaxation of $OD(A\,^2\Sigma^+, v = 2)$ by O_2, obtained $k(2 \rightarrow 0)/k(2 \rightarrow 1) = 1/10$, a small fraction.

Finally, we interpret our results in the context of the Schwartz, Slawsky, Herzfeld (SSH) theory[33] for vibrational relaxation. The large energy difference between any of the $OH^\dagger$ frequencies—$\nu(1) = 3570$ cm^{-1}, $\nu(9) = 2237$ cm^{-1}—and the O_2 frequency of 1554 cm^{-1} makes resonant V–V transfer *via*

$$OH(v) + O_2(0) \rightarrow OH(v-1) + O_2(1)$$

infeasible. The low efficiencies obtained here (0.1%) are also indicative of relaxation which does not use a resonant V–V mechanism. Since we are unable to probe the vibrational quantum state of the O_2 product, we cannot distinguish a V–T from a non-resonant V–V mechanism. For either mechanism, however, SSH theory predicts (1) rate constants for single-quantum relaxation which increase linearly with v, and (2) double-quantum relaxation rates which are 3 orders of magnitude smaller than the single-quantum rates. Both predictions are consistent with our experimental results. Although we obtain good fits to the data using a single-quantum model, we cannot draw any conclusions concerning the precise importance of a double-quantum mechanism. SSH theory fails when strong intermolecular interactions occur between the vibrationally excited molecule and relaxer molecule, as is the case at low temperatures (< 200 K), or when both species are strongly polar. Such interactions are not expected in the present system.

We believe that our ability to obtain both time and spectrally resolved emission data of high S/N which can be analyzed using standard spectral fitting techniques represents a valuable tool for the deciphering of molecular relaxation problems. In particular, our overall picture of $OH^\dagger$ decay kinetics complements the more detailed laser-induced fluorescence techniques currently under development for the study of high v $OH^\dagger$.[34] We plan to extend our studies of $OH^\dagger$ collisional relaxation to other relaxer molecules, including Ar, NO, and N_2O.

ACKNOWLEDGMENTS

We thank Dr. B. David Green of Physical Sciences Inc. for very useful discussions. J.A.D. acknowledges the support of a Geophysics Scholarship (1988–89), administered by the Southeastern Center for Electrical Engineering Education, and sponsored by the Air Force Office of Scientific Research (AFOSR). This research was supported separately by the AFOSR under Task No. 2310G4 and by the Defense Nuclear Agency under Project SA, Task SA 'Nuclear Backgrounds, Work Unit 0213.

[1] J. G. Anderson, Geophys. Res. Lett. **3**, 165 (1976).
[2] I. C. McDade, E. J. Llewellyn, D. P. Murtagh, and R. G. H. Greer, Planet. Space Sci. **35**, 1137 (1987).
[3] A. B. Meinel, Astrophys. J. **111**, 555 (1950).
[4] G. E. Caledonia, B. D. Green, and R. E. Murphy, J. Chem. Phys. **71**, 4369 (1979).
[5] R. E. Murphy, E. T. P. Lee, and A. M. Hart, J. Chem. Phys. **63**, 2919 (1975).
[6] K. G. Anlauf, R. G. MacDonald, and J. C. Polanyi, Chem. Phys. Lett. **1**, 619 (1968).
[7] L. Mertz, Infrared Phys. **7**, 17 (1967).
[8] R. E. Murphy, J. Chem. Phys. **54**, 4852 (1971).
[9] J. A. Coxon, Can. J. Phys. **58**, 933 (1980).
[10] J. A. Coxon and S. C. Foster, Can. J. Phys. **60**, 41 (1982).
[11] F. H. Mies, J. Molec. Spectrosc. **53**, 150 (1974).
[12] S. R. Langhoff, H.-J. Werner, and P. Rosmus, J. Molec. Spectrosc. **118**, 507 (1986).
[13] D. N. Turnbull and R. P. Lowe, Planet. Space Sci. **37**, 723 (1989).
[14] D. D. Nelson, Jr., A. Schiffman, and D. J. Nesbitt, J. Chem. Phys. **90**, 5455 (1989); D. D. Nelson, Jr., A. Schiffman, D. J. Nesbitt, J. Orlando, J. R. Burkholder and C. J. Howard (submitted).
[15] D. N. Turnbull and R. P. Lowe, J. Chem. Phys. **89**, 2763 (1988).
[16] D. J. Flanagan (unpublished).
[17] W. H. Press, B. P. Flannery, S. A. Teukolsky, and W. T. Vetterling, *Numerical Recipes* (Cambridge University Press, New York, 1986).
[18] D. L. Thompson, J. Phys. Chem. **86**, 2538 (1982).
[19] D. L. Thompson, Chem. Phys. Lett. **92**, 383 (1982).
[20] G. D. Greenblatt and J. R. Wiesenfeld, J. Geophys. Res. **87**, 11 145 (1982).
[21] T. G. Slanger and D. L. Huestis, Int. J. Chem. Kin. **17**, 713 (1985).
[22] B. D. Green, G. E. Caledonia, W. A. M. Blumberg, and F. H. Cook, J. Chem. Phys. **80**, 773 (1984).
[23] J. E. Spencer and G. P. Glass, Chem. Phys. **15**, 35 (1976).
[24] B. J. Finlayson-Pitts and T. E. Kleindienst, J. Chem. Phys. **74**, 5643 (1981).
[25] G. K. Smith and J. E. Butler, J. Chem. Phys. **73**, 2243 (1980); J. E. Butler, G. M. Jursich, I. A. Watson, and J. R. Wiesenfeld, *ibid.* **84**, 5365 (1986).
[26] R. F. Heidner III and D. Husain, Int. J. Chem. Kinet. **6**, 77 (1974) measured a rate constant of $7.1(\pm 13)$ cm^3/s for $O(^1D)$ quenching by Ar. Later experiments, however, suggest a value a factor of 2 lower than this,

see, e.g., J. A. Davidson, C. M. Sadowski, H. I. Schiff, G. E. Streit, C. J. Howard, D. A. Jennings, and A. L. Schmeltekopf, J. Chem. Phys. **64**, 57 (1976). We use this lower value.
[27]S. T. Amimoto, A. P. Force, R. G. Gulotty, Jr., and J. R. Wiesenfeld, J. Chem. Phys. **71**, 3640 (1979).
[28]D. H. Jaffer and I. W. M. Smith, Faraday Discuss. Chem. Soc. **67**, 212 (1979).
[29]K. J. Rensberger, J. B. Jeffries, and D. R. Crosley, J. Chem. Phys. **90**, 2174 (1989).
[30]G. E. Streit and H. S. Johnston, J. Chem. Phys. **64**, 95 (1976).
[31]J. Burris, J. J. Butler, T. J. McGee, and W. S. Heaps, Chem. Phys. **124**, 251 (1988), and references therein.
[32]K. R. German, J. Chem. Phys. **64**, 4065 (1976).
[33]J. D. Lambert, *Vibrational and Rotational Relaxation in Gases* (Clarendon, Oxford, 1977).
[34]A. D. Sappey, D. R. Crosley, and R. A. Copeland, J. Chem. Phys. **90**, 3484 (1989).